POLITECNICO DI TORINO
Repository ISTITUZIONALE

Glass-ceramics for joining oxide-based ceramic matrix composites (Al2O3/Al2O3-ZrO2) operating under direct flame exposure

(Article begins on next page)

20 March 2024

Glass-ceramics for joining oxide-based ceramic matrix composites (Al_2O_{3f}/Al_2O_3-ZrO_2) operating under direct flame exposure

Carla Malinverni [a,*], Milena Salvo [a], Alessandro De Zanet [a], Fabiana D'Isanto [a], Federico Smeacetto [a], Pierre Bertrand [b], Georg Puchas [c], Stefan Schafföner [c], Valentina Casalegno [a]

[a] *Department of Applied Science and Technology, Politecnico di Torino, Corso Duca degli Abruzzi 24, 10129 Torino, Italy*
[b] *University Bourgogne Franche-Comté, Laboratory ICB, UMR - 6303 CNRS, site UTBM, 90010 Belfort, France*
[c] *Chair of Ceramic Materials Engineering, University of Bayreuth, Prof.-Rüdiger-Bormann-Str. 1, 95447 Bayreuth, Germany*

ARTICLE INFO

ABSTRACT

This work focuses on the joining processes of oxide-based ceramic matrix composites (Al_2O_{3f} /Al_2O_3-ZrO_2), which are used as radiant tube furnace components in the steel industry. These components have to operate in harsh environments, and under high temperatures, and they therefore have to resist corrosion, humidity, and combustion. Two glass-ceramics systems, which have $Y_2Ti_2O_7$ as their main crystalline phase, as well as specific and optimized properties to withstand severe operating conditions, including temperatures of 900 °C, are here proposed as joining materials. The adhesion of the glass-ceramics to the composite was found to be excellent after mechanical and thermal tests in which they were in direct contact with a 900 °C flame and thermal cycling of between 400 °C and 900 °C.

1. Introduction

Over the last few years, the ecological transition of the steel industry has been a major subject of interest. One of the main goals of this energy-intensive sector is to improve the relevant production processes to lower carbon emissions, and to decrease the associated energy input by using renewable energy sources. Thus, radiant tube furnaces are increasingly being manufactured with innovative and high-performance materials, such as ceramic matrix composites (CMCs), in order to obtain environmentally and economically sustainable steel production.

Because of their exceptional properties, ceramic matrix composites are currently being used as high-performance materials for applications under severe conditions, including high temperatures, corrosive environments, high levels of humidity and other demanding requirements [1–4]. Oxide/oxide ceramic matrix composites (Ox-CMCs), which belong to this class of materials, are composed of oxide fibers with an oxide matrix. Oxide/oxide CMCs are characterized by their intrinsic oxidation resistance, good thermal shock resistance, lower density and lower cost than non-oxide CMCs [5]. Their applications range from the production of furnace components, flame tubes and hot gas distributors [5] to aero-engines [6,7]. CMCs can be used to substitute metallic

components in all the aforementioned applications, as metallic components may fail to operate under such challenging conditions.

This work focuses on the joining of oxide/oxide CMCs, which are used in the energy-intensive steel industry for radiant tube furnaces. The main goals have been to increase the lifetime of the tubes, to improve their energy efficiency and to reduce CO_2 emissions by using clean and renewable energy. Oxide/oxide CMCs are chosen to substitute the Inconel/stainless steel alloys that are currently used to manufacture comparable components. Establishing the joining capability of these composites is essential to validate the possibility of using oxide/oxide CMCs in radiant tube furnaces. The successful joining of oxide/oxide CMCs at high temperatures (up to 800 °C) with glass-ceramics and brazing alloys was reported in previous studies, from both the mechanical and thermal stability points of view [8–10]. The joined CMCs showed good adhesion and uniform interfaces after thermal aging, with higher flexural strength of the joints after heat treatment, and good oxidation resistance when joined with glass-ceramics.

A sustainable steel production requires very high temperatures (up to 900 °C). Furthermore, in such a production, the components are in contact with green fuels that contain mixtures of hydrogen and biogas. Therefore, the joints may need to endure excessive wear and corrosion,

Table 1
Chemical compositions, in weight percentages, of the T1 and T2M glasses.

	T1	T2M
SiO_2 [wt%]	30.91	30.91
Al_2O_3 [wt%]	20.60	20.60
TiO_2 [wt%]	20.60	15.60
Y_2O_3 [wt%]	15.46	11.70
CaO [wt%]	5.15	9.53
Na_2O [wt%]	5.15	2.13
K_2O [wt%]	2.13	9.53

Table 2
Joining processes performed for the T1 and T2M joints.

Glass	T1	T2M
Heat treatment (heating and cooling rate of 10 °C/min)	● 1300 °C, 10 min + 855 °C, 30 min under flowing Ar ● 1200 °C, 10 min + 855 °C, 30 min under flowing Ar or air	● 1250 °C, 10 min + 960 °C, 30 min under flowing Ar

hydrothermal attacks, and degradation after long exposure times. The joining materials should have a similar coefficient of thermal expansion (CTE) to that of oxide/oxide CMCs, and they should be thermodynamically stable. Moreover, they should be thermo-mechanically and chemically compatible with the oxide/oxide CMCs and show good wettability on the composites [8].

Several studies have reported on the use of glass-ceramics as joining materials for ceramics and CMCs, for example, for Nextel™ 610/Al₂O₃-ZrO₂ CMC [8,9], Nextel™ 610/YAG-ZrO₂ CMC [10], alumina-to-alumina and mullite-to-SiC joints [11], SiC/SiC and C/SiC joints [12], Si₃N₄-to-porous Si₃N₄ joints [13], and sealants in solid oxide fuel/electrolysis cell stacks [14,15]. They have also been used as environmental barrier coatings for non-oxide and oxide/oxide CMCs [16, 17].

Glass-ceramics are often chosen as joining materials because of their tunable chemical composition and properties. These properties include their characteristic temperatures, CTE, and crystalline phases, as well as their ability to join complex geometries and to resist severe environments. They can be used as self-healing materials when operating at temperatures above the softening temperature, since they can repair cracks generated during the service life [12,18]. Their production consists of melting raw powders of a tailored composition, and then casting the thus obtained molten glass. Subsequently, the as-cast glass undergoes a thermal treatment whereby the process of sinter-crystallization occurs, and a glass-ceramic material is obtained. The crystallization process can in particular improve the refractoriness and creep resistance of the glass-ceramics [19].

In this work, two silica-based glass-ceramic systems have been characterized in depth as joining materials of oxide/oxide CMCs that can be used as radiant tubes in the steel industry.

2. Materials and methods

2.1. Oxide/oxide ceramic matrix composites

The oxide/oxide ceramic matrix composite was supplied by the Chair of Ceramic Materials Engineering at the University of Bayreuth, Germany. It consisted of an alumina-zirconia matrix (75 wt% alumina and 25 wt% zirconia) reinforced with eight layers of Nextel™ 610 alumina fiber fabric DF-19 (8 Harness Satin, 3000 denier). The oxide/oxide CMC had a fiber volume content of about 42% and a porosity of around 27%. The CMC was manufactured by means of a prepreg process, using glycerol to adjust the water content and the tack of the prepregs, a process that has already been described in detail [20,21]. The interlaminar shear strength (ILSS) of this system was in the 12 MPa range, with a 3-point flexural strength of around 400 MPa, and a tensile strength of about 300 MPa. The coefficients of thermal expansion (CTE) were: $8.2 \bullet 10^{-6}$ °C^{-1} (125–500 °C) and $8.6 \bullet 10^{-6}$ °C^{-1} (125–1200 °C).

2.2. Glass-ceramics and joining processes

The composition of the two glass-based joining materials was designed by resorting to the SciGlass 6.6 software database. The thermal expansion and the glass transition temperature (T_g) predicted by the software were the main parameters that were considered. The glass

referred to as T1 had previously been developed by D'Isanto et al., and it had been used as an oxidation protective coating for a titanium suboxide thermoelectric material [22]. The glass referred to as T2M contained the same oxides as T1, but with different weight percentages, although the same TiO_2/Y_2O_3 ratio was kept to obtain $Y_2Ti_2O_7$ as the main crystalline phase after the devitrification process. Starting from the known T1 glass composition and properties, the T2M glass was designed to obtain lower characteristic temperatures so as to allow joining to take place at lower temperatures.

The compositions of the T1 and T2M glasses are summarized in Table 1.

SiO_2 (99.5%, Sigma Aldrich), Al_2O_3 (99.9%, Alfa Aesar), TiO_2 ($\geq$ 99%, Sigma Aldrich), Y_2O_3 (99.99%, Sigma Aldrich), $CaCO_3$ (99%, Sigma Aldrich), Na_2CO_3 (99.5%, Sigma Aldrich) and K_2CO_3 (99.5%, Sigma Aldrich) were used as high-purity grade precursors. They were weighed and mixed on a roller shaker for 1 day. The powders were first melted in a platinum-rhodium crucible at 1500 °C for 1 h before they were heated to 1550 °C for 30 min in an electric furnace (Nabertherm GmbH, Germany). They were then air quenched on a brass plate, according to the procedure described in Reference [22]. To obtain the glass powders, the as-cast glasses underwent milling and sieving processes, which yielded a final maximum particle size of less than 38 μm.

Both glass powders were characterized using differential thermal analysis (DTA 404 PC, Netzsch, Germany) and heating-stage microscopy (HSM, Hesse Instruments, Germany) with an image analysis system (EM 301, Hesse instruments, Germany). The DTA was carried out in air using alumina powder as a reference, starting from room temperature and going up to 1300 °C, at a heating rate of 10 °C/min.

The HSM was carried out in air by placing the glass pellet on an alumina plate and heating it from room temperature up to 1300 °C, at a heating rate of 10 °C/min.

In this work, the joining technique consisted of a slurry deposition. For this purpose, the T1 and T2M glass powders (70 vol%), respectively, were dispersed in ethanol (30 vol%) and placed between two oxide/oxide CMC pieces, using a spatula. A flat-joint and a butt-joint configuration were used as two different setups to evaluate the infiltration of the glass-ceramic in regard to the orientation of the composite fibers. Two different joining processes were carried out for the T1 glass. The first one consisted of a heating step at 1300 °C for 10 min, followed by a heat treatment at 855 °C for 30 min under an Ar flow, at a heating and cooling rate of 10 °C/min. The second joining process was carried out at 1200 °C for 10 min, followed by a heat treatment at 855 °C for 30 min under flowing Ar or air, at a heating and cooling rate of 10 °C/min. T2M underwent a joining process at 1250 °C for 10 min, followed by a heat treatment at 960 °C for 30 min under flowing Ar, at a heating and cooling rate of 10 °C/min. The joining processes performed for T1 and T2M are summarized in Table 2.

Fig. 1 shows the typical joints that were obtained, and indicative dimensions of the two different joining configurations, where the average thickness of the glass-ceramic layer was around ~200–300 μm.

The crystalline phases that formed within the glass T1 and T2M during the joining processes were analyzed by means of X-ray diffraction (XRD) with a Malvern PANalytical X'Pert PRO diffractometer and the support of X-Pert HighScore Software. Morphological and compositional characterizations of the joints and the glass-ceramics were conducted
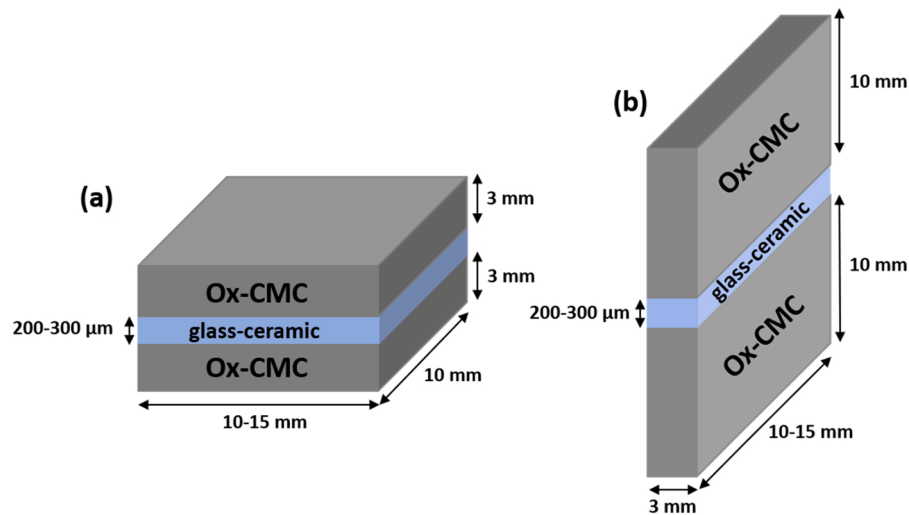
Fig. 1. The two different joining configurations for the glass-ceramic joined oxide/oxide CMCs: (a) flat-joint configuration and (b) butt-joint configuration.
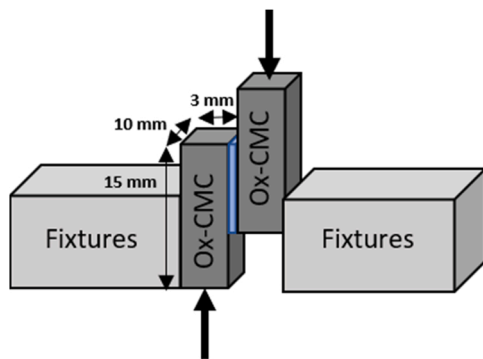

Fig. 2. Single lap offset (SLO) test.

Table 3
Thermal tests conducted on the T1 and T2M glass-ceramic pellets (Test 1) and joints (Test 2). The conditions and the duration of the tests are reported.

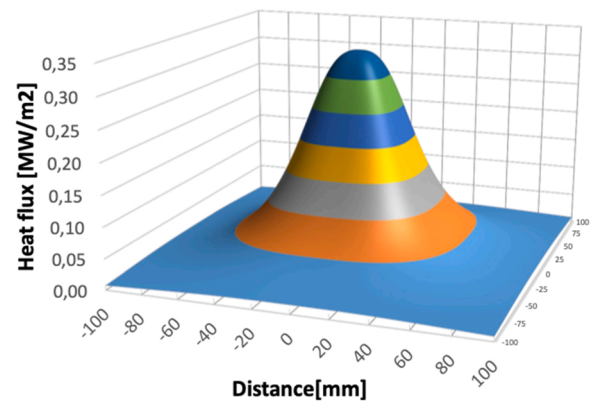| Thermal tests conducted by means of direct flame exposure	
TEST 1	**TEST 2**
C_2H_2/O_2 flame at 900 °C for 30 min on T1 and T2M glass-ceramic pellets	C_2H_2/O_2 flame at 900 °C for 30 min + 10 cycles 400 °C → 900 °C on T1 and T2M joints

Fig. 3. Estimated heat flux generated by the flame on the surface of the samples during the flame test.

using scanning electron microscopy (SEM, JCM-6000Plus, JEOL) and field emission scanning electron microscopy (FE-SEM, Merlin electron microscope, ZEISS, Germany). Energy dispersive X-ray spectrometry (EDS) was utilized for the elemental mapping (Supra TM 40, ZEISS, Germany) of the glass-ceramic crystalline phases. The coefficients of thermal expansion of T1 and T2M were investigated for both the as-cast glasses and glass-ceramics, after the joining process, using dilatometry (DIL, 402 PC, Netzsch, Germany) in air up to 1300 °C at a heating rate of 5 °C/min.

The apparent shear strength of the glass-ceramic joined oxide/oxide CMCs was measured on three samples for each glass-ceramic by means of a compressive single lap offset (SLO) test. The SLO test was carried out at room temperature, using a universal testing machine (SINTEC D/10). A 50 kN load cell was utilized and the crosshead speed was set at 0.5 mm/min. The maximum force was recorded, and the apparent shear strength was calculated by dividing the maximum force by the joining area (Fig. 2). Further information on the SLO set-up is available in Reference [10].

The flexural strength of the as-received and of the heat-treated at the joining conditions oxide/oxide CMCs was measured in a 3-point bending test adapted from the ASTM C1341–13 standard at room temperature, using a universal testing machine (MTS Criterion MODEL 43, US) with a crosshead speed of 0.2 mm/min. The used sample measured 50 mm × 5 mm × 3 mm, and the support span was 40 mm.

Furthermore, two thermal tests were conducted, by means of direct flame exposure, at the University of Bourgogne Franche-Comté, France, to evaluate the behavior of the glass-ceramics and glass-ceramic joined oxide/oxide CMCs in the combustion environment.

The goal was to investigate whether this environment could affect the morphology and thermomechanical properties of the joining material, i.e., thermomechanical stress on the samples, and any possible reactions at the interface between the oxide/oxide CMC and the joining material. Table 3 summarizes the conditions of the direct thermal flame exposure tests conducted on the T1 and T2M samples. In the first test, a T1 glass-ceramic pellet (sintered at 1300 °C, 10 min; 855 °C, 30 min, Ar, to test the most challenging conditions) and a T2M glass-ceramic pellet (sintered at 1250 °C, 10 min; 960 °C, 30 min, Ar) were positioned directly in front of an oxy-acetylenic C_2H_2/O_2 900 °C flame (stoichiometric ratio) for 30 min. By assuming the combustion reaction was complete at the point of impact of the flame with the sample, the partial pressure of water vapor can reach up to 30 kPa. The distance between the flame and the sample was adjusted to reach a surface temperature of 900 °C, which was controlled by a thermal camera (Flir systems). Under
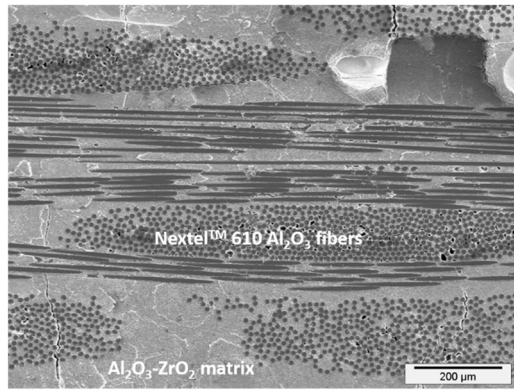
Fig. 4. Microstructure of the Nextel™ 610 $Al_2O_{3\,f}$ /Al_2O_3-ZrO_2 CMC obtained from the scanning electron microscopy. It is possible to distinguish both the matrix and the fibers of the composite.

these conditions, the heat flux generated by the flame on the surface of the samples was estimated, using a home-made calorimeter, as being around 0.33 MW/m², as depicted in Fig. 3.

The second test was conducted to evaluate the behavior of the glass-ceramic oxide/oxide CMC joints under thermal cycling. A flat-joint configuration, with one side exposed to the flame, was used to be representative of the application. After a dwell time of 30 min in front of a C_2H_2/O_2 900 °C flame, 10 cycles were performed between 400 °C and 900 °C, with average heating and cooling rates of around 10–12 °C/s, followed by natural air cooling. The treated samples were analyzed by means of scanning electron microscopy, whereas the XRD analyses were carried out on the flame-tested T1 and T2M glass-ceramic pellets used in Test 1.

3. Results and discussion

A cross-section showing the microstructure of the oxide/oxide CMC is depicted in Fig. 4. The Al_2O_3-ZrO_2 matrix and Nextel™ 610 Al_2O_3 fibers can be observed.

The T1 glass system was fully characterized as a coating material in a

previous study [22], and its DTA and HSM curves are reported in Fig. 5 for comparison with the ones obtained for the as-cast T2M.

The dilatometric analyses showed that the as-cast T1 had a CTE of $8.6 \cdot 10^{-6}$ °C^{-1} (200–500 °C) and a dilatometric softening point at ~792 °C [22], while the CTE of the as-cast T2M glass was $10.4 \cdot 10^{-6}$ °C^{-1} (200–500 °C), and the dilatometric softening point was ~834 °C.

The joining temperatures of the two systems were selected considering the results of the DTA and HSM analyses in order to perform the joining processes at the lowest possible temperature to avoid any thermal degradation of the oxide/oxide CMCs.

3.1. T1 glass-ceramic

Two different joining heat treatments were used for the T1 glass, as reported in the Materials and Methods section. The two sintering processes were carried out on the T1 powder pellets (~ 5 mm thickness and 10 mm diameter). It was found, from the dilatometric analyses of the two sintered T1 glass-ceramic pellets and the as-cast T1, that the CTE of T1 increased slightly after the heat treatments, i.e., from $8.6 \cdot 10^{-6}$ °C^{-1} to $9.4 \cdot 10^{-6}$ °C^{-1} (200–500 °C) for sintering at 1300 °C, and to $9.6 \cdot 10^{-6}$ °C^{-1} (200–500 °C) for sintering at 1200 °C. As previously observed [22], the dilatometric softening temperature increased significantly from 792 °C, for the parent glass, to ~1110 °C for the glass-ceramics.
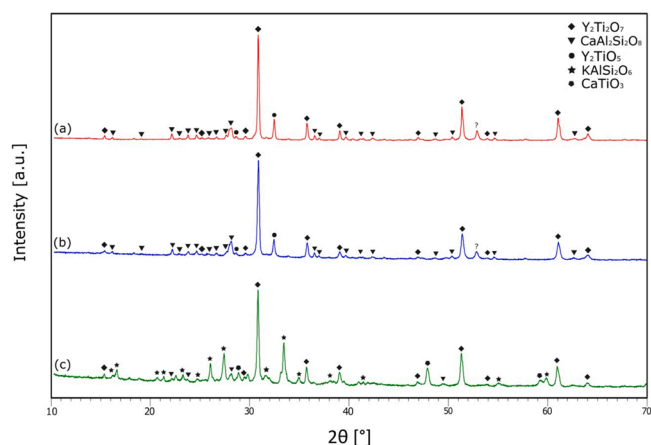
The XRD patterns of the T1 glass-ceramic sintered at 1300 °C (already reported and discussed in Reference [22]) and at 1200 °C are shown in Fig. 6a-b. Along with the residual glassy phase, the cubic pyrochlore $Y_2Ti_2O_7$ phase was the main crystalline phase that was present after both thermal treatments, whereas $CaAl_2Si_2O_8$ (anorthite) and Y_2TiO_5 were detected as secondary phases in both samples. The comparison shows a very good match between the two patterns for the different treatments, and the same crystalline phases can be observed.

Fig. 7a shows the cross-section of the T1 butt-joint obtained from the heat treatment at 1300 °C under flowing Ar, i.e., above the T1 melting point. The glass-ceramic presented homogeneously distributed crystalline phases and low porosity, which were in agreement with the previously reported microstructure [22]. Furthermore, it was possible to observe an infiltration of T1 into the oxide/oxide CMC porosity, which can be noticed by a dark contrast at the T1/composite interface. For this
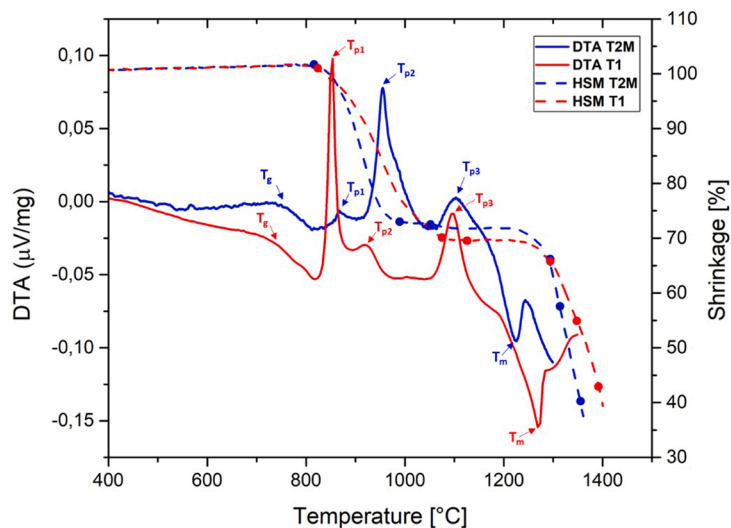
Fig. 5. The DTA and HSM curves obtained for the as-cast T1 [22] and T2M glasses with a particle size < 38 μm. The characteristic DTA temperatures are reported: glass transition temperature (Tg), crystallization temperature peak 1 (Tp1). crystallization temperature peak 2 (Tp2), crystallization temperature peak 3 (Tp3), and melting temperature (Tm). The characteristic points obtained from HSM are reported in ascending order: first shrinkage temperature (TFS), maximum shrinkage temperature (TMS), deformation temperature (DT), spherical temperature (ST), hemispherical temperature (HT), and flow temperature (FT).

| Glass	T_g	T_{p1}	T_{p2}	T_{p3}	T_m	TFS	TMS	DT	ST	HT	FT
T1	752°C	852°C	919°C	1097°C	1271°C	835°C	1080°C	1126°C	1294°C	1342°C	1394°C
T2M	765°C	867°C	955°C	1103°C	1226°C	820°C	976°C	1055°C	1294°C	1318°C	1352°C

Fig. 6. Comparison between the XRD patterns for the T1 glass-ceramic heat-treated at 1300 °C, 10 min + 855 °C, 30 min under flowing Ar (a), the T1 glass-ceramic heat-treated at 1200 °C, 10 min + 855 °C, 30 min under flowing Ar (b), and the T2M glass-ceramic heat-treated at 1250 °C, 10 min + 960 °C, 30 min under flowing Ar (c). The identified crystalline phases were $Y_2Ti_2O_7$ (PDF card no.00–042–0413), $CaAl_2Si_2O_8$ (PDF card no. 00–041–1486), Y_2TiO_5 (PDF card no. 00–027–0981) and $KAlSi_2O_6$ (PDF card no.01–085–1626), and $CaTiO_3$ (PDF card no.01–077–0182).

heat treatment, the microstructure of the glass-ceramic (Fig. 7d) was characterized by the presence of small uniform grains (~0.8–1 μm) of the main crystalline phase, $Y_2Ti_2O_7$, which were incorporated and surrounded by the amorphous phase.

The cross-section of a T1 butt-joint, obtained from the heat treatment at 1200 °C under flowing Ar (T < T1 melting temperature), is shown in Fig. 7b. The infiltration of the glass-ceramic at the oxide/oxide CMC surface was very limited and, despite the similarity of the XRD patterns (Fig. 6a-b), the T1 microstructure appeared quite different. The T1 glass-ceramic that sintered at 1200 °C showed large pores, which were non-homogeneously distributed, as well as the presence of a large amount of the residual glassy phase and areas where a phase separation of the T1 glass was clearly detectable (brighter areas in Fig. 7e). Moreover, the compromise that was adopted for the process temperature between the viscosity of the glass-ceramic and pore coalescence might have influenced the formation of gas bubbles. Because of the intrinsic oxidation resistance of the oxide/oxide CMCs, the joining process at 1200 °C was also conducted in static air. The cross-section of the joints manufactured in static air (Fig. 7c) revealed a high porosity and a lack of adhesion at the T1/ composite interface, while the microstructure (Fig. 7f) was the same as that of the heat treatment up to 1200 °C under flowing Ar. It has been speculated that the joining process carried out under flowing Ar led to a lower porosity than that formed when processing in air, because the gas entrapped in the glass powder and/or due to the oxide/oxide CMC degassing at high temperature was more easily transported from the
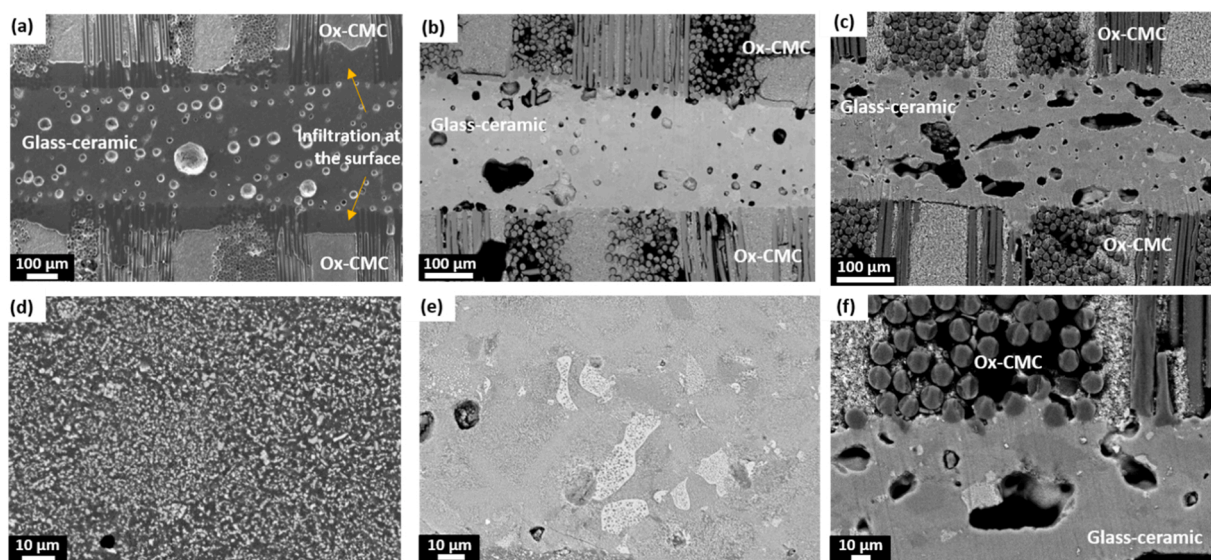
Fig. 7. SEM cross-sections of the butt-joint configuration for the T1 glass-ceramic oxide/oxide CMC joints heat-treated under different conditions: (a, d) 1300 °C, 10 min + 855 °C, 30 min under flowing Ar, (b, e) 1200 °C, 10 min + 855 °C, 30 min under flowing Ar, (c, f) 1200 °C, 10 min + 855 °C, 30 min in air. Images a, b, and c show the joining area with the glass-ceramic layers, while images d, e, and f show the microstructure of the glass-ceramics near the interface under a higher magnification. Images a and d are obtained in SE mode, while images b, c, e and f are obtained in BSE mode.
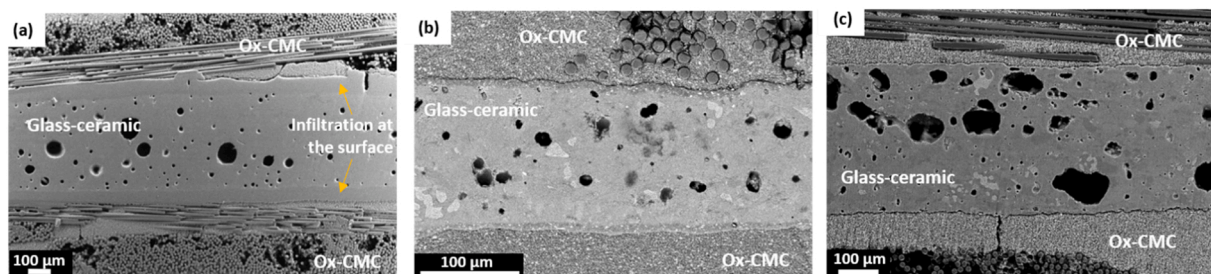
Fig. 8. SEM cross-sections of the flat-joint configuration for the T1 glass-ceramic oxide/oxide CMC joints heat-treated under different conditions: (a) 1300 °C, 10 min + 855 °C, 30 min under flowing Ar, (b) 1200 °C, 10 min + 855 °C, 30 min under flowing Ar, (c) 1200 °C, 10 min + 855 °C, 30 min in air. Images a, b, and c show the joining area with the glass-ceramic layers and are obtained in BSE mode.
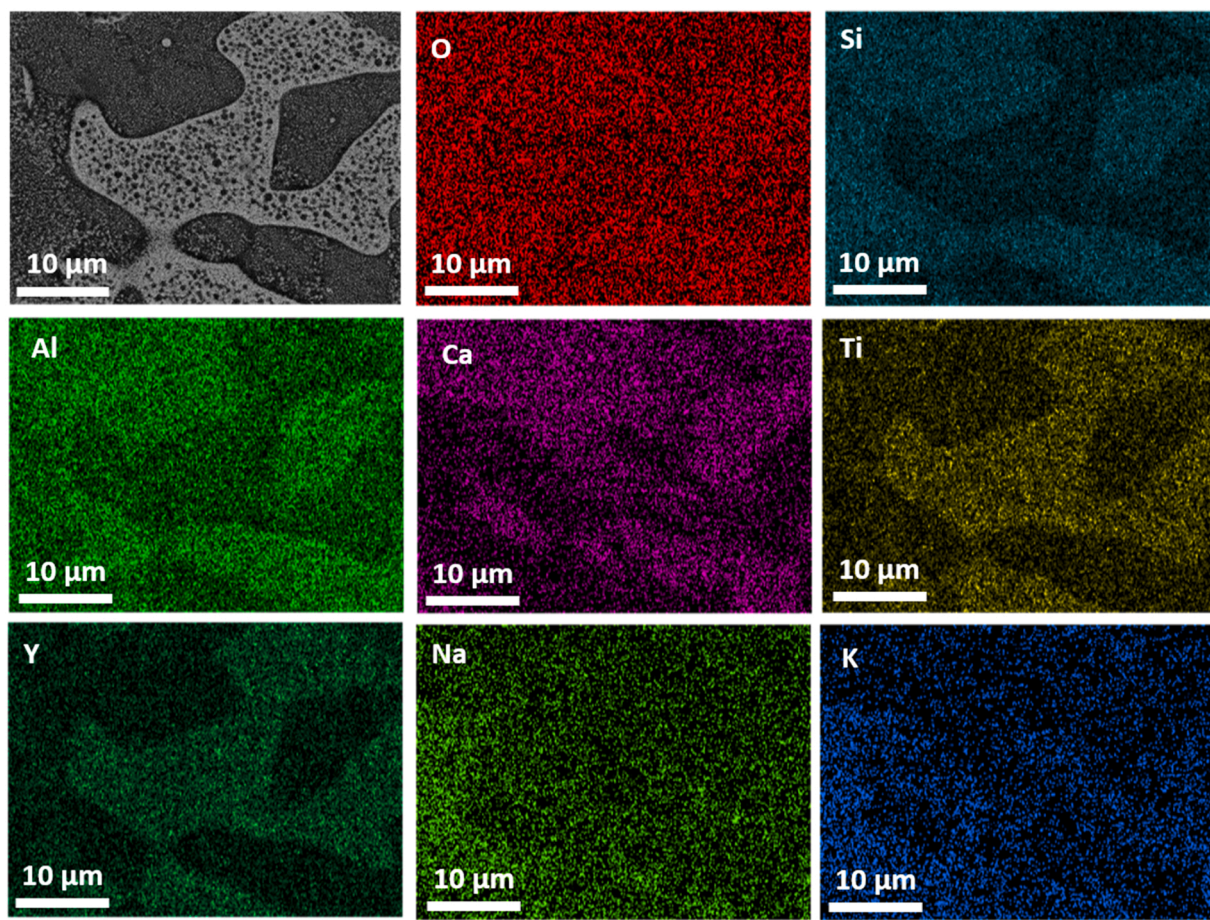
Fig. 9. EDX elemental maps of the T1 glass-ceramic pellet heat-treated at 1200 °C, 10 min + 855 °C, 30 min under flowing Ar.

surface by the Ar flux. The cross-sections of the T1 flat-joints presented in Fig. 8 show no significant differences between the butt-joint and flat-joint configurations. Regardless of the fiber orientation in the CMC, the joint interfaces exhibited the same morphology, and no cracks were detected in the glass-ceramic joining material, which demonstrates the good CTE match between the T1 glass-ceramic and the oxide/oxide CMC.

EDS elemental maps of the T1 glass-ceramic pellets obtained after the two heat treatments at 1300 °C and 1200 °C were acquired to further investigate the difference in the glass-ceramic microstructure. After the heat treatment at 1300 °C, it was possible to identify small grains of the $Y_2Ti_2O_7$ pyrochlore phase. The Ca rich elongated crystals can be attributed to the $CaAl_2Si_2O_8$ anorthite phase, and they were identified by means of XRD, TEM and SAED analyses in Ref. [22]; a residual

amorphous phase remained. Fig. 9 shows a magnification and the related elemental maps of the T1 glass-ceramic sintered at 1200 °C, where a darker region with small $Y_2Ti_2O_7$ grains embedded in the glassy matrix surrounds a region of glass-phase separation, which probably caused the formation of glass droplets. Primary $Y_2Ti_2O_7$ crystals formed in these glass droplets, in a similar way to what was previously discussed for the as-cast T1 [22–24].

On the basis of the above results, 1300 °C for 10 min, followed by a heat treatment at 855 °C for 30 min (heating and cooling rate of 10 °C/min) under flowing Ar were chosen for joining heat treatment for the T1 joined oxide/oxide CMCs.
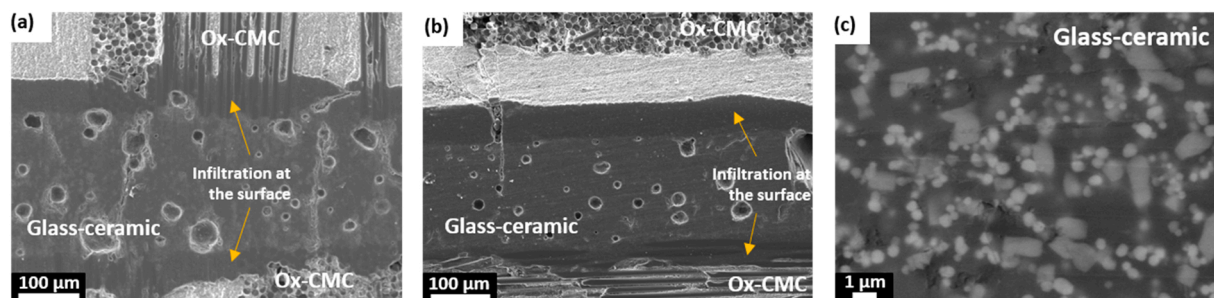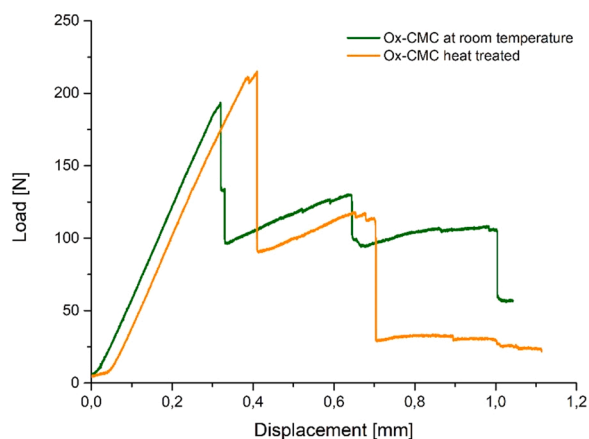

Fig. 10. SEM cross-sections of the butt-joint (a) and flat-joint (b) configurations for the T2M glass-ceramic oxide/oxide CMC joints heat-treated at 1250 °C, 10 min + 960 °C, 30 min under flowing Ar. Images a and b show the joining area with the glass-ceramic layers, while image c reports the microstructure of the glass-ceramic. Images a, b and c are obtained in SE mode.

Fig. 11. 3-point bending tests for the oxide/oxide ceramic matrix composites for the two different treatments: as-received (green curve) and after the heat treatment at 1300 °C, 10 min + 855 °C, 30 min under flowing Ar (orange curve). The two characteristic curves reported in the figure were obtained for the two different conditions.

3.2. T2M glass-ceramic

Considering the DTA and HSM results, a sinter-crystallization process at 1250 °C for 10 min, followed by a heat treatment at 960 °C for 30 min under flowing Ar was selected for T2M. The same heat treatment was used for the joining process of the oxide/oxide CMCs with T2M. Similarly to T1, T2M showed a CTE increase after the sinter-crystallization heat treatment (from $10.4 \bullet 10^{-6} °C^{-1}$ to $12.3 \bullet 10^{-6} °C^{-1}$ between 200 °C and 500 °C) and a significant increase in its refractoriness, with a softening point at ~1165 °C, which was more than 300 °C higher than that of the T2M parent glass.

The XRD pattern of the T2M glass-ceramic heat-treated at 1250 °C for 10 min, followed by 960 °C for 30 min under flowing Ar, is depicted in Fig. 6c, where a slight change, compared to the XRD patterns of the T1 glass-ceramic, can be noticed for a few peaks. However, this glass-ceramic still contained $Y_2Ti_2O_7$ as the main crystalline phase, while the other crystalline phases that were present were $CaAl_2Si_2O_8$, $KAlSi_2O_6$ (leucite) and $CaTiO_3$.

The CMC/T2M/CMC joints heat-treated at 1250 °C for 10 min, followed by 960 °C for 30 min under flowing Ar, were obtained for the T2M glass, and the micrographs of the cross-sections are reported in Fig. 10a-b for the butt-joint (a) and flat-joint (b) configurations. The T2M/CMC interface was continuous, and the good wettability of the glass-ceramic allowed it to infiltrate into the porosity of the oxide/oxide CMC. The T2M microstructure in Fig. 10c appears homogeneous and has a low porosity. In this case, though, the higher CTE value of the T2M glass-ceramic, compared to those of the oxide/oxide CMC, may explain

the presence of some vertical cracks that can be observed along the glass-ceramic layer.

3.3. Mechanical characterizations

In order to evaluate the effect of the joining heat treatment on the mechanical properties of the composite, three-point bending tests were carried out on the as-received and heat-treated oxide/oxide CMCs. The oxide/oxide CMCs were heat-treated by means of the same joining process as T1 (1300 °C for 10 min followed by 855 °C for 30 min, Ar), but at a higher temperature than the T2M process. Two of the typical load-displacement curves that were obtained are shown in Fig. 11. The flexural strength of the as-received and heat-treated oxide/oxide CMCs was 245 ± 26 MPa and 309 ± 8 MPa, respectively, and the quasi-ductile behavior of the composite was preserved after the thermal treatment. The higher flexural strength of the heat-treated samples suggested that densification of the alumina-zirconia matrix might have occurred during the heat treatment.
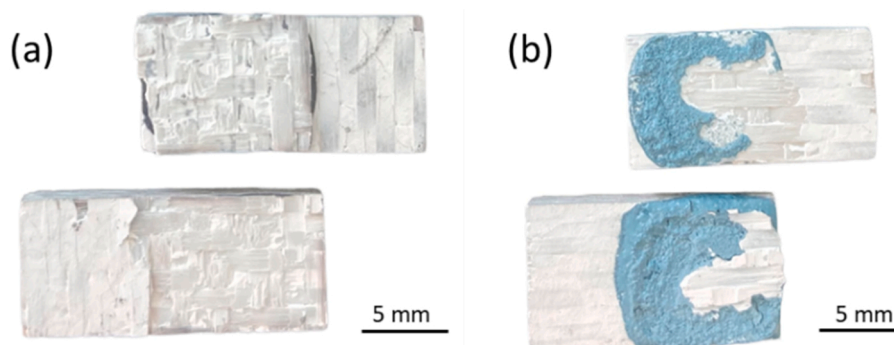
Furthermore, single lap shear offset tests were performed on the T1 and T2M joints for the CMC/glass-ceramic/CMC flat configuration. This test is recommended when comparing the joining strength of a set of samples [10]. The measured values of the apparent shear strength were 18 ± 5 MPa and 12 ± 5 MPa for the T1 joints and T2M joints, respectively. These values are comparable with the interlaminar strength of the oxide-based composite, which is around 12 MPa [20]. The fracture surfaces of the T1 and T2M joints, after the single lap shear offset tests, are depicted in Fig. 12. It is possible to notice the delamination of the oxide/oxide CMC for the T1 joints (Fig. 12a), while the failure mode for the T2M joints is partially cohesive within the glass-ceramic, and delamination of the composite can be observed (Fig. 12b). Thus, the micrographs prove the higher bonding strength of T1 joints than of T2M joints.

As a result of the mismatch of the T2M and oxide/oxide CMC thermal expansion, the joining process created higher stresses in the T2M joints than in the T1 joints. These stresses then caused the formation of the cracks observed in the glass-ceramic (Fig. 10), which were able to coalesce and propagate during the lap shear test, thus reducing the strength of the T2M joined components.

3.4. Direct flame exposure tests

Two different thermal tests were conducted, by means of direct flame exposure, to evaluate the behavior of the glass-ceramics and glass-ceramic joined oxide/oxide CMCs in a combustion environment.

Test 1 was performed by placing T1 and T2M glass-ceramic pellets directly in front of a 900 °C C_2H_2/O_2 flame for 30 min. The T1 pellet showed no change in mass after Test 1, whereas the T2M pellet exhibited a mass loss of 0.3 mg. Test 2 was aimed at analyzing the behavior of the glass-ceramic oxide/oxide CMC joints under thermal cycling to check


Fig. 12. Single lap shear offset tests for the (a) T1 and (b) T2M joints. The T1 joint shows delamination of the oxide/oxide CMC, while the T2M joint shows mixed adhesive-cohesive failure.
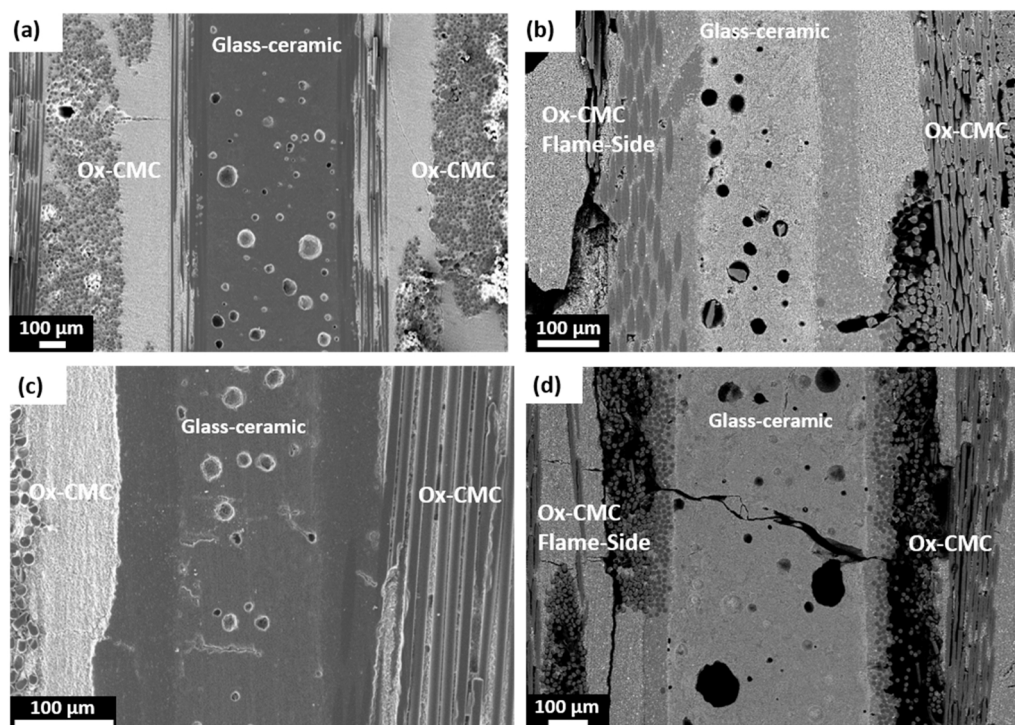
Fig. 13. Cross-sections of the T1 oxide/oxide CMC joints and the T2M oxide/oxide CMC joints before (a, c) and after (b, d) the flame post-treatment (Test 2), respectively. In the SEM images, it is possible to notice some cracks across the T2M joints, while no cracks are observed on the T1 glass-ceramic layer. Images a and c are obtained in SE mode, while Images b and d are obtained in BSE mode.
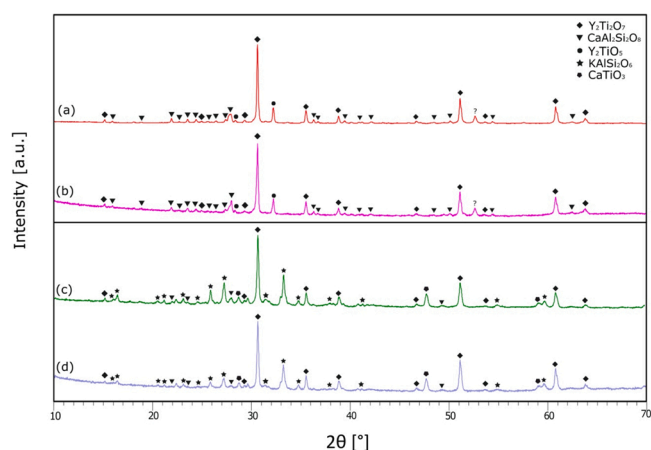
Fig. 14. Comparison between XRD patterns of T1 glass-ceramic pellets heat-treated at 1300 °C, 10 min + 855 °C, 30 min under flowing Ar, before (a), after flame test with oxy-acetylenic flame (b), and XRD patterns of T2M glass-ceramic pellets heat-treated at 1250 °C, 10 min + 960 °C, 30 min under flowing Ar, before (c), after flame test with oxy-acetylenic flame (d).

whether the evolution of the joining material could promote cracks under thermomechanical stress. Under these conditions, the joined samples were subjected to thermo-mechanical stress resulting from the gradient temperature between the two faces of the samples. After the treatments, some cracks appeared on the outer surfaces of the composites, especially in the area in contact with the flame, but no delamination was observed. The cross-sections of the oxide/oxide CMC surfaces directly in contact with the flame, as observed by means of SEM, are shown in Fig. 13 before (Fig. 13a-c) and after the treatment (Fig. 13b-d) of the T1 and T2M joints, respectively. The T2M joints show vertical cracks across the glass-ceramic layer, which are not observed for the T1 joints, thus indicating an excellent thermal cycling resistance of the T1

glass-ceramic under the extreme conditions of this test.

XRD analyses were carried out on the T1 and T2M glass-ceramic pellets after the first flame test with the oxy-acetylenic flame. The XRD patterns did not show any change for either glass-ceramic after the tests, when compared with the as-sintered pellets (Fig. 14). No modification in the crystalline structure of the glass-ceramics was detected with this technique when the sample was treated in a combustion environment.

4. Conclusions

Two glass-ceramics have been designed to join an Al_2O_{3f}/Al_2O_3-ZrO_2 composite that operates at temperatures of up to 900 °C in combustion environments. The heat treatments that were selected for the joining processes led to glass-ceramics with improved refractory properties, e.g. an increase of ~300 °C in the dilatometric softening temperature was observed after devitrification of both parent glasses.

Furthermore, the mechanical tests on the as-received and heat-treated oxide/oxide CMCs confirmed that their mechanical properties were not affected by the thermal treatments of the joining processes. The T1 joints showed an apparent higher shear strength than the interlaminar shear strength of the composites, which led to failure of the composites during the single-lap offset tests.

Preliminary direct-flame and thermal cycling tests were carried out on both the glass-ceramics and joined samples. Neither the T1 nor the T2M glass-ceramics showed a relevant mass loss, and no delamination was observed at the glass-ceramics/ oxide/oxide composite interface after exposure to such relevant conditions as flame tests at 900 °C and thermal cycling between 400 °C and 900 °C. An excellent thermal cycling resistance was observed of the T1 glass-ceramic joined composites between 400 °C and 900 °C.

Declaration of Competing Interest

The authors declare that they have no known competing financial

interests or personal relationships that could have appeared to influence the work reported in this paper.

Acknowledgments

References

[1] A. Sommers, Q. Wang, X. Han, C. T'Joen, Y. Park, A. Jacobi, Ceramics and ceramic matrix composites for heat exchangers in advanced thermal systems-A review, Appl. Therm. Eng. 30 (2010) 1277–1291, https://doi.org/10.1016/j.applthermaleng.2010.02.018.

[2] R. Naslain, Design, preparation and properties of non-oxide CMCs for application in engines and nuclear reactors: an overview, Compos. Sci. Technol. 64 (2004) 155–170, https://doi.org/10.1016/S0266-3538(03)00230-6.

[3] N. Radhika, M. Sathish, A review on Si-based ceramic matrix composites and their infiltration based techniques, Silicon 14 (2022) 10141–10171, https://doi.org/10.1007/s12633-022-01763-y.

[4] T. Nallusamy, S. Vijayakumar, Reinforcements, manufacturing techniques, and respective property changes of Al_2O_3/SiC based composites: a review, Silicon 14 (2022) 3129–3146, https://doi.org/10.1007/s12633-021-01108-1.

[5] W. Pritzkow, A. Nöth, A. Rudinger, Oxide ceramic matrix composites – manufacturing, machining, properties and industrial application, Ceram. Appl. 3 (2015).

[6] G. G. Karadimas, K. Salonitis, K. Georgarakis, Oxide ceramic matrix composite materials for aero-engine applications: a literature review, Adv. Manuf. XXXIV (2021), https://doi.org/10.3233/ATDE210029.

[7] S. Datta, S. Das, A new high temperature resistant glass–ceramic coating for gas turbine engine components, Bulletin of Material, Science 28 (2005) 689–696, https://doi.org/10.1007/BF02708539.

[8] M.Y. Akram, V. Casalegno, M. Ferraris, G. Puchas, W. Krenkel, S. Roszeitis, Joining and mechanical testing of oxide/oxide (Nextel™ 610/alumina zirconia) ceramic composites, J. Eur. Ceram. Soc. 39 (2019) 2510–2517, https://doi.org/10.1016/j.jeurceramsoc.2019.02.020.

[9] M. Ferraris, S. De la Pierre, Y. Akram, C. Steinborn, G. Puchas, W. Krenkel, High temperature creep behaviour of glass-ceramic joined Nextel 610™/ Al_2O_3-ZrO_2 composites, J. Eur. Ceram. Soc. 42 (2022) 5029–5034, https://doi.org/10.1016/j.jeurceramsoc.2022.04.052.

[10] M.Y. Akram, M. Ferraris, V. Casalegno, M. Salvo, G. Puchas, S. Knohl, W. Krenkel, Joining and testing of alumina fibre reinforced YAG-ZrO_2 matrix composites,

[11] J. Eur. Ceram. Soc. 38 (2018) 1802–1811, https://doi.org/10.1016/j.jeurceramsoc.2017.11.026.

[11] P.K. Gianchandani, V. Casalegno, S. De la Pierre des Ambrois, M. Salvo, G. De Aloysio, L. Laghi, M. Ferraris, Joining of SiC, alumina, and mullite by the Refractory Metal—Wrap pressure-less process, Int. J. Appl. Ceram. Technol. 17 (2020) 980–989, https://doi.org/10.1111/ijac.13477.

[12] F. Smeacetto, F. D'Isanto, V. Casalegno, P. Tatarko, M. Salvo, Ytterbium disilicate-based glass-ceramic as joining material for ceramic matrix composites, J. Eur. Ceram. Soc. 41 (2021) 1099–1106, https://doi.org/10.1016/j.jeurceramsoc.2020.10.022.

[13] L. Sun, J. Fang, S. Guo, Joining dense Si_3N_4 to porous Si_3N_4 using a novel glass-ceramic interlayer with precipitated β-$LiAlSi_2O_6$/Mg_2SiO_4, J. Eur. Ceram. Soc. 42 (2022) 87–95, https://doi.org/10.1016/j.jeurceramsoc.2021.09.050.

[14] A.G. Sabato, G. Cempura, D. Montinaro, A. Chrysanthou, F. Smeacetto, M. Secco, F. Smeacetto, Glass-ceramic sealant for solid oxide fuel cells application: Characterization and performance in dual atmosphere, J. Power Sources 328 (2016) 262–270, https://doi.org/10.1016/j.jpowsour.2016.08.010.

[15] M. Ferraris, S. De la Pierre, A.G. Sabato, F. Smeacetto, H. Javed, C. Walter, J. Malzbender, Torsional shear strength behavior of advanced glass-ceramic sealants for SOFC/SOEC applications, J. Eur. Ceram. Soc. 40 (2020) 4067–4075, https://doi.org/10.1016/j.jeurceramsoc.2020.04.034.

[16] C. Gatzen, D. Mack, O. Guillon, R. Vaßen, $YAlO_3$—A Novel Environmental Barrier Coating for Al_2O_3/ Al_2O_3–Ceramic Matrix Composites, Coatings 9 (2019) 609, https://doi.org/10.3390/coatings9100609.

[17] E. García, A. Nistal, F. Martín de la Escalera, A. Khalifa, M.A. Sainz, M.I. Osendi, P. Miranzo, Thermally Sprayed Y_2O_3- Al_2O_3-SiO_2 Coatings for High-Temperature Protection of SiC Ceramics, J. Therm. Spray. Technol. 24 (2015) 185–193, https://doi.org/10.1007/s11666-014-0178-y.

[18] M. Salvo, F. Smeacetto, F. D'Isanto, G. Viola, P. Demitri, F. Gucci, M.J. Reece, Glass-ceramic oxidation protection of higher manganese silicide thermoelectrics, J. Eur. Ceram. Soc. 39 (2019) 66–71, https://doi.org/10.1016/j.jeurceramsoc.2018.01.007.

[19] M. Ferraris, V. Casalegno, F. Smeacetto, M. Salvo, Glass as a joining material for ceramic matrix composites: 25 years of research at Politecnico di Torino, Int. J. Appl. Glass Sci. 11 (2020) 569–576, https://doi.org/10.1111/ijag.15032.

[20] G. Puchas, S. Möckel, W. Krenkel, Novel prepreg manufacturing process for oxide fiber composites, J. Eur. Ceram. Soc. 40 (2020) 5930–5941, https://doi.org/10.1016/j.jeurceramsoc.2020.06.064.

[21] F. Lindner, G. Puchas, S. Schafföner, Novel measuring method for prepreg processability of oxide fiber ceramic matrix composites, Compos. Part A: Appl. Sci. Manuf. 162 (2022), 107131, https://doi.org/10.1016/j.compositesa.2022.107131.

[22] F. D'Isanto, F. Smeacetto, H.-P. Martin, R. Sedlák, M. Lisnichuk, A. Chrysanthou, M. Salvo, Development and characterisation of a $Y_2Ti_2O_7$- based glass-ceramic as a potential oxidation protective coating for titanium suboxide (TiO_x), Ceram. Int. 47 (2021) 19774–19783, https://doi.org/10.1016/j.ceramint.2021.03.316.

[23] T. Wei, Y. Zhang, L. Kong, Y.J. Kim, A. Xu, I. Karatchevtseva, N. Scales, D.J. Gregg, Hot isostatically pressed $Y_2Ti_2O_7$ and $Gd_2Ti_2O_7$ pyrochlore glass-ceramics as potential waste forms for actinide immobilization, J. Eur. Ceram. Soc. 39 (2019) 1546–1554, https://doi.org/10.1016/j.jeurceramsoc.2018.11.012.

[24] L. Kong, Y. Zhang, I. Karatchevtseva, Preparation of $Y_2Ti_2O_7$ pyrochlore glass-ceramics as potential waste forms for actinides: the effects of processing conditions, J. Nucl. Mater. 494 (2017) 29–36, https://doi.org/10.1016/j.jnucmat.2017.07.004.